Correction Factor on Dynamic Force in a Marsh Funnel Test for Tunneling

Zheng, Dongzhu; Bezuijen, Adam; Talmon, Arno

DOI
10.1061/(ASCE)GM.1943-5622.0002439

Publication date
2022

Document Version
Final published version

Published in
International Journal of Geomechanics

ASCE

Correction Factor on Dynamic Force in a Marsh Funnel Test for Tunneling

Dongzhu Zheng[1]; Adam Bezuijen[2]; and Arno Talmon[3]

Abstract: This paper presents an improvement on a previous model for predicting the Marsh funnel (MF) test that is used in slurry shield tunneling for evaluating the rheological properties of bentonite slurries. The improvement focuses on the prediction of the dynamic part for fluids with small MF times. The velocity profile of the Herschel–Bulkley fluid in a laminar pipe flow condition is first investigated and a correction factor is introduced in the improved model. Comparisons of results from experiments and calculations with the previous model confirm the improved performance over the existing model. The rheological parameters obtained from the improved model show good resemblance to those obtained from a laboratory viscometer. The work also provides a reference to similar applications such as fluid transportation through pipelines where dynamic pressure dominates and therefore should be correctly predicted considering its velocity profile in a laminar condition. **DOI: 10.1061/(ASCE)GM.1943-5622.0002439**. © *2022 American Society of Civil Engineers*.

Author keywords: Correction factor; Marsh funnel test; Bentonite slurry; Rheology; Field use.

Introduction

The Marsh funnel (MF) is an inexpensive testing device for field use that avoids complex testing equipment and tedious lab work. It is applied in tunneling for evaluation of the bentonite slurries that are used for face support in slurry shield tunneling and has recently been interpreted by model studies (Schoesser and Thewes 2015; Zheng et al. 2021). The expected MF viscosity for slurries used in tunneling is relatively small for the American Petroleum Institute (API RP 13B-1, API 2009) recommended funnel geometry [Fig. 1(a)]. In this test, the funnel is filled with 1,500 mL of fluid and the time it takes for one quart (946 mL) of that fluid to drain is recorded as the MF viscosity.

Balhoff et al. (2011) developed a new calculation model describing non-Newtonian fluid flow through a Marsh funnel. Rheological parameters can be obtained by fitting the measured volume against time data to the model. However, for fluids with a small MF viscosity, the dynamic pressure becomes dominant and should be included in model studies. Based on the Herschel–Bulkley model, Zheng et al. (2021) established a new model, using the flow description from Skelland (1967), and also considering the pressure drop in the conical section of the funnel due to the presence of the yield stress and the dynamic pressure in the capillary tube which is the pressure drop necessary to accelerate the fluid from hardly any velocity in the funnel to the outflow velocity. Results suggest the feasibility of the Zheng et al. (2021) model, especially for low viscosity fluids in tunneling applications.

[1]Dept. of Civil Engineering, Ghent Univ., Technologiepark 68, Ghent 9052 Belgium (corresponding author). ORCID: https://orcid.org/0000-0002-7570-2125. Email: zhengdongzhu.geo@gmail.com

[2]Dept. of Civil Engineering, Ghent Univ., Technologiepark 68, Ghent 9052, Belgium; Deltares, Delft 2600 MH, Netherlands. ORCID: https://orcid.org/0000-0002-5591-0461

[3]Dept. of Dredging Engineering, Delft Univ. of Technology, Mekelweg 2, 2628 Delft; Deltares, Delft 2600 MH, Netherlands.

Note. This manuscript was submitted on November 8, 2021; approved on February 22, 2022; published online on July 6, 2022. Discussion period open until December 6, 2022; separate discussions must be submitted for individual papers. This paper is part of the ***International Journal of Geomechanics***, © ASCE, ISSN 1532-3641.

The rheological properties such as yield stress and viscosity could influence the infiltration behavior of bentonite slurries into saturated sand due to the stress–strain behaviors of different materials (Xu and Bezuijen 2019; Xiao et al. 2020; Zheng 2021). As an inexpensive device frequently used in field testing, the potential of using the MF test to obtain more information on the slurries is of great interest.

For bentonite slurries, the rheological behavior can be described by the Herschel–Bulkley model (API 2009), which consists of three parameters: yield stress (τ_0), consistency index (C), and flow index (n). The Herschel–Bulkley model can describe a lot of fluid models (Newtonian, Power law, and Bingham, and so on, see Schoesser and Thewes 2015) and it is described as follows:

$$\tau = \tau_0 + C\dot{\gamma}^n \tag{1}$$

where τ = shear stress; τ_0 = yield stress; and $\dot{\gamma}$ = shear rate.

The major advantage of the Zheng et al. (2021) model compared with the Balhoff et al. (2011) model is the inclusion of the dynamic pressure as well as the squeezing pressure in the conical section of the funnel. The relation between the dynamic part and the mean velocity in Zheng et al. (2021) is

$$p = \frac{1}{2}\rho\bar{v}^2 \tag{2}$$

where p = dynamic pressure; ρ = density of the fluid; and $\bar{v}$ = mean velocity.

Since there will be shearing behavior among the streamlines of the flow, the velocity in the cross section of the tube will be a function of the radial distance from the center to the walls. This uneven distribution will make a difference when a mean velocity is considered in Eq. (2) for the calculation of the dynamic part because the square of the mean velocity is different from the integral of the square of its components under such conditions.

This paper presents an improvement on the previous model by Zheng et al. (2021). The improvement focuses on the treatment of the square value of the velocity in the capillary tube. The velocity profile of the Herschel–Bulkley fluid in a fully developed pipe flow condition is first investigated. A correction factor in relation to the square value of the velocity is included in the improved model for the dynamic part. Sensitivity analysis is performed to investigate the

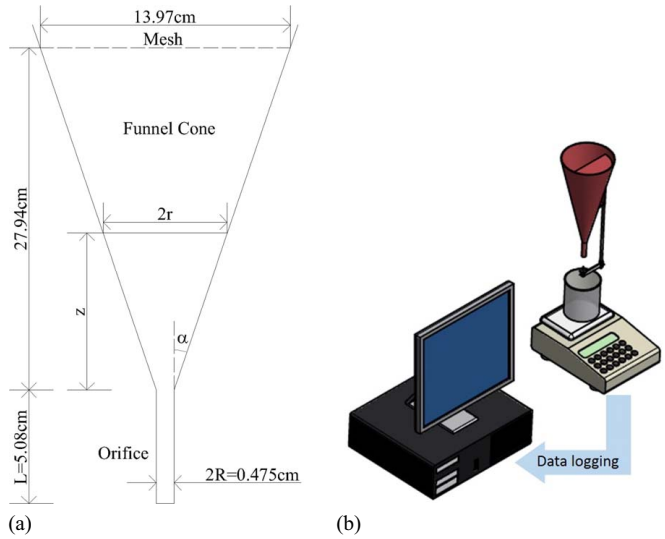

Fig. 1. Marsh funnel: (a) dimensions according to API (2009); and (b) the testing system. (Reprinted from Zheng et al. 2021, © ASCE.)

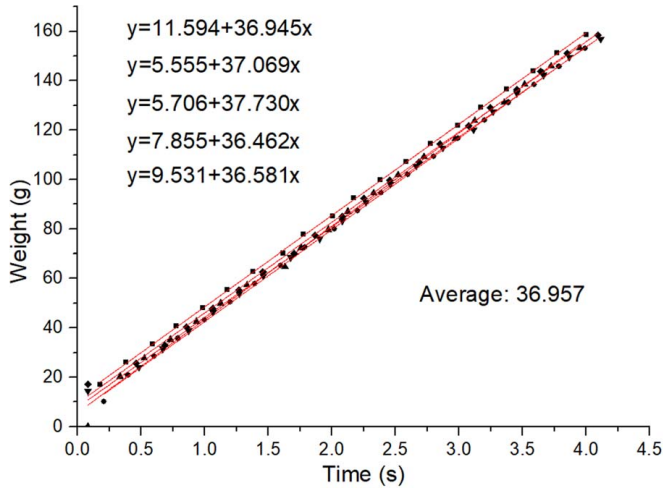

Fig. 2. Measurement data for water during the first 4 s of the test and the average discharge rate.

influence of the rheological parameters of the fluids. Comparisons with experimental and previous model results are conducted.

Flow Condition in the Tube of the Marsh Funnel

In the previous model (Zheng et al. 2021), the flow in the capillary tube is assumed to be a laminar flow, because the discharge rate can be explicitly derived under such conditions. While it is necessary to show that the fluid in the capillary tube during the MF test is a laminar flow. To start with, the Reynolds number (Re) is

$$\mathrm{Re} = \frac{QD\rho}{\mu A} \tag{3}$$

where Q = discharge rate; D = diameter of the pipe; μ = viscosity; and A = cross-sectional area of the pipe.

The discharge rate in the first few seconds of such a test can be estimated to be a linear discharge as suggested by the measurement data in Zheng et al. (2021). Since the discharge rate will slowly

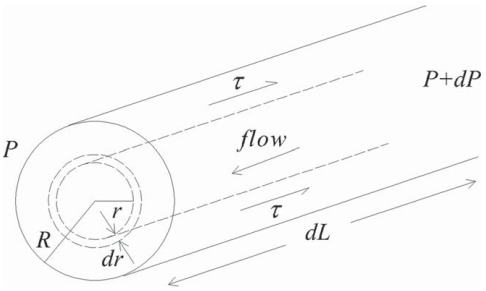

Fig. 3. Herschel–Bulkley fluid in a pipe flow.

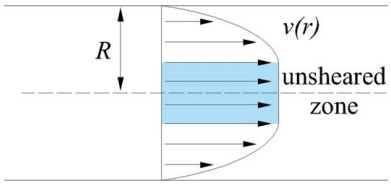

Fig. 4. 2D velocity profile of a Hershel–Bulkley fluid in a fully developed pipe flow.

decrease with elapsed time, there will be a decreasing trend in the Reynolds number. Therefore, it will be a laminar flow condition if the calculated Reynolds number in the beginning of the test is smaller than 2,300.

Fig. 2 shows the linear fit of the measured discharge in the first 4 s for water. The average value of the slope is taken to be the discharge rate and the Reynolds number can be calculated to be about 9,906. However, since it is an acceleration flow, the critical Reynolds number could be much higher than 2,300 (Knisely et al. 2010).

For other tested fluids, the viscosity is calculated with the model by Pitt (1999).

$$\mu = \frac{\rho}{10^6}(t - 25) \tag{4}$$

where t = measured MF time.

The discharge rate can be estimated with the measured MF time assuming a discharge of 946 mL of liquid at a constant drainage rate, which is a reasonable assumption as shown by the measurement curves in Zheng et al. (2021) for low viscosity fluids.

Adding Eq. (4) into Eq. (3), we obtain

$$\mathrm{Re} = \frac{10^6 VD}{\mathrm{At}(t - 25)} \tag{5}$$

where V = drainage volume of 946 mL.

It can be found with Eq. (5) that the Reynolds number is smaller than 2,300 when $t \geq 29$ s, suggesting a laminar condition for the tested bentonite slurries as shown in Zheng et al. (2021). Since the focus of the study is on testing bentonite slurries with an MF time larger than 30 s, the laminar condition should be investigated based on the above analysis.

Velocity Profile in a Herschel–Bulkley Pipe Flow

For a fully developed flow condition in the capillary tube, the pressure drop due to viscous force along the flow direction will be linearly distributed. It will be an axisymmetric flow along the centerline of the pipe.

Fig. 3 shows a schematic view of a portion of the fluid flow from the center of the pipe. For laminar conditions, there is the following

relation:

$$\pi r^2 dP = 2\pi r \tau dL \tag{6}$$

where r = radius of the portion of the fluid; P = fluid pressure (corrected for height here in the MF test); and L = length of the fluid.

The following relation can be obtained:

$$\tau = \frac{r}{2}\frac{dP}{dL} \tag{7}$$

When $\tau \le \tau_0$, there will be no shearing among the fluid, thus there is an unsheared zone in the fluid, with the previous equation the radius of the unsheared zone (r_0) is

$$r_0 = 2\tau_0 \left(\frac{dP}{dL}\right)^{-1} \tag{8}$$

To initiate the flow, there should be such a relation $r_0 \le R$. The minimum pressure gradient is

$$\frac{dP}{dL} = \frac{2\tau_0}{R} \tag{9}$$

where R = radius of the pipe.

For pipe flow, the shear rate ($\dot{\gamma}$) can be described as follows:

$$\dot{\gamma} = -\frac{dv}{dr} \tag{10}$$

where v = fluid velocity.

Combining Eqs. (1), (7), and (10), the following yields:

$$-\frac{dv}{dr} = \frac{1}{C^{(1/n)}}\left(\frac{r}{2}\frac{dP}{dL} - \tau_0\right)^{(1/n)} \tag{11}$$

By integration, the following is obtained:

$$v = -\frac{1}{C^{(1/n)}}\int\left(\frac{r}{2}\frac{dP}{dL} - \tau_0\right)^{(1/n)} dr \tag{12}$$

Note that there is boundary condition when $r = R$, $v = 0$ and when $r \le r_0$, $v = v$ ($r = r_0$), the the following velocity profile is obtained:

$$v = \begin{cases} \dfrac{2}{C^{(1/n)}((1/n)+1)\left(\frac{dP}{dL}\right)}\left[\left(\frac{R}{2}\left(\frac{dP}{dL}\right) - \tau_0\right)^{(1/n)+1} - \left(\frac{r}{2}\left(\frac{dP}{dL}\right) - \tau_0\right)^{(1/n)+1}\right] & r_0 \le r \le R \\ \dfrac{2}{C^{(1/n)}((1/n)+1)\left(\frac{dP}{dL}\right)}\left[\left(\frac{R}{2}\left(\frac{dP}{dL}\right) - \tau_0\right)^{(1/n)+1} - \left(\frac{r_0}{2}\left(\frac{dP}{dL}\right) - \tau_0\right)^{(1/n)+1}\right] & 0 \le r \le r_0 \end{cases} \tag{13}$$

Fig. 4 shows the 2D velocity profile according to Eq. (13). In general, the velocity is zero at the edges of the pipe and increases toward the center. There is an unsheared zone around the centerline of the pipe. Outside this unsheared zone, the velocity profile is nonlinearly distributed.

The discharge rate of the pipe flow is of interest since the dynamic part in the MF test is directly related to it, as shown in Eq. (2). With Eq. (13), it is possible to get the discharge rate.

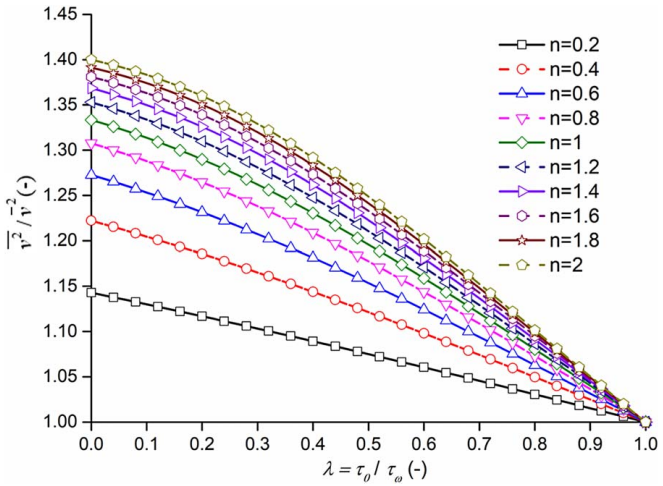

Fig. 5. Relation between the correction factor and the ratio of yield stress and wall shear stress for fluids with different fluid index (n).

Fig. 3 also shows the schematic view of a sleeve of the fluid in the pipe flow from the center of the pipe. The discharge rate of the sleeve is

$$dQ = 2\pi r v dr \tag{14}$$

Integration from 0 to R and add it into Eq. (13), the discharge rate across the entire pipe is

$$Q = \frac{\pi R^3\left(\frac{R}{2}\left(\frac{dP}{dL}\right) - \tau_0\right)^{(1/n)+1}}{C^{(1/n)}\left(\frac{R}{2}\left(\frac{dP}{dL}\right) - \tau_0\right)^3} \times \left[\frac{\left(\frac{R}{2}\left(\frac{dP}{dL}\right) - \tau_0\right)^2}{(1/n)+3} + \frac{2\tau_0\left(\frac{R}{2}\left(\frac{dP}{dL}\right) - \tau_0\right)}{(1/n)+2} + \frac{\tau_0^2}{(1/n)+1}\right] \tag{15}$$

Note that when $r = R$, the shear stress becomes the wall shear stress (τ_w):

$$Q = \frac{\pi R^3(\tau_w - \tau_0)^{(1/n)+1}}{C^{(1/n)}\tau_w^3}\left[\frac{(\tau_w - \tau_0)^2}{(1/n)+3} + \frac{2\tau_0(\tau_w - \tau_0)}{(1/n)+2} + \frac{\tau_0^2}{(1/n)+1}\right] \tag{16}$$

Which is the same to that shown by Skelland (1967).

The following mean velocity can be obtained with Eq. (16):

$$\overline{v} = \frac{R(\tau_w - \tau_0)^{(1/n)+1}}{C^{(1/n)}\tau_w^3}\left[\frac{(\tau_w - \tau_0)^2}{(1/n)+3} + \frac{2\tau_0(\tau_w - \tau_0)}{(1/n)+2} + \frac{\tau_0^2}{(1/n)+1}\right] \tag{17}$$

Correction Factor for the Dynamic Part

In the work of Zheng et al. (2021), Eq. (7) was extended to include the dynamic part, resulting in the wall shear stress described as follows:

$$\tau_w = 0.5\frac{R}{L}\left[\Delta P_{tot} - \frac{1}{2}\rho\left(\frac{Q}{\pi R^2}\right)^2\right] \tag{18}$$

The discharge rate and the wall shear stress in the capillary tube in their study were obtained through iteration due to the implicit relation between Eqs. (16) and (18). However, in the dynamic part [the second term on the right-hand side of Eq. (18)], the square of the mean velocity is not equal to the integral of the square of its components.

The square of the mean velocity can be obtained with Eq. (17):

$$\overline{v}^2 = \frac{R^2(\tau_w - \tau_0)^{(2/n)+2}}{C^{(2/n)}\tau_w^2}\left[\frac{1}{((1/n)+3)^2} + \frac{4\lambda}{((1/n)+2)((1/n)+3)^2} + \frac{4((2/n)+3)\lambda^2}{((1/n)+1)((1/n)+2)^2((1/n)+3)^2} + \frac{8\lambda^3}{((1/n)+1)((1/n)+2)^2((1/n)+3)^2} + \frac{4\lambda^4}{((1/n)+1)^2((1/n)+2)^2((1/n)+3)^2}\right] \tag{19}$$

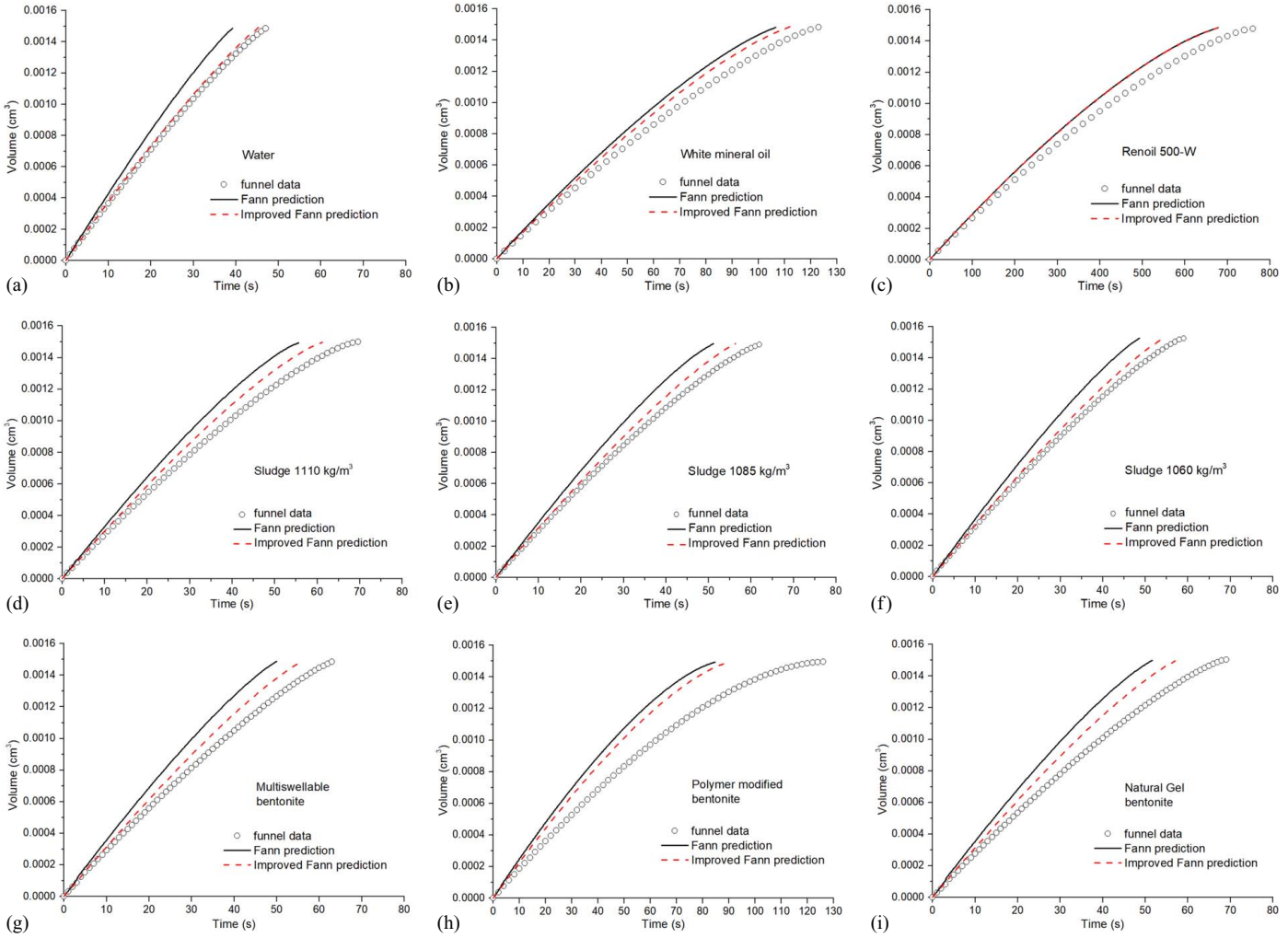

Fig. 6. Volume versus time data for: (a) water; (b) white mineral oil; (c) Renoil 500-W; (d) Sludge 1,110 kg/m^3; (e) Sludge 1,085 kg/m^3; (f) Sludge 1,060 kg/m^3; (g) multiswellable bentonite; (h) natural gel bentonite; and (i) polymer-modified bentonite compared with model results. [Data for (a–c; g–i) from Zheng et al. 2021.]

Table 1. Parameters used in model predictions

Fluid	τ_0 (Pa)	τ_w (Pa)	n (—)	Range for λ (—)	Range for correction factor	Correction factor
Water	0	—	1	0	1.33	1.33
White mineral oil[a]	0	—	1	0	1.33	1.33
Renoil 500-W[a]	0	—	1	0	1.33	1.33
Sludge 1,110 kg/m^3[a]	6	15–31	1	0.19–0.4	1.23–1.29	1.26
Sludge 1,085 kg/m^3	3.5	13–26	1	0.13–0.27	1.27–1.31	1.29
Sludge 1,060 kg/m^3	2.5	16–22	1	0.11–0.16	1.30–1.31	1.30
Multiswellable bentonite	0.26	14–26	0.88	0.01–0.02	1.32	1.32
Natural gel bentonite[a]	1.72	15–26	0.7	0.07–0.11	1.27–1.28	1.28
Polymer modified bentonite[a]	1.51	22–50	0.6	0.03–0.07	1.26–1.27	1.27

[a]Source: Data from Zheng et al. (2021).

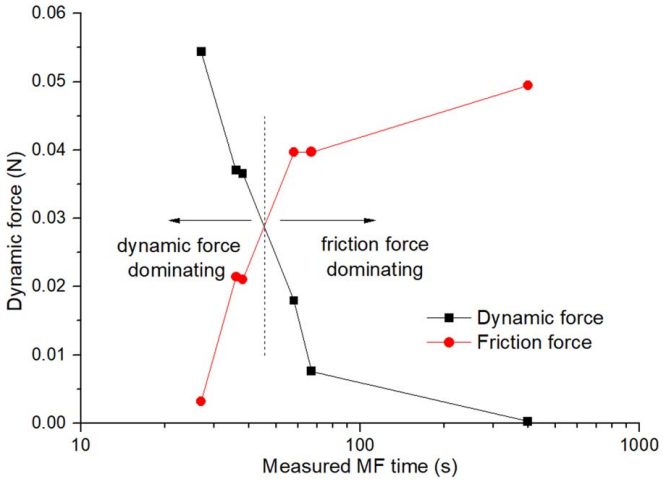

Fig. 7. Comparison between dynamic force and friction force. (Reprinted from Zheng et al. 2021, © ASCE.)

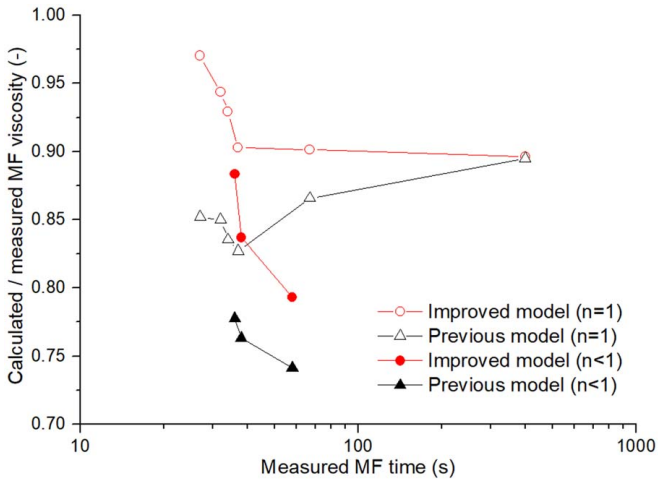

Fig. 8. Prediction ratio as a function of the measured MF time.

where λ = ratio between the yield stress (τ_0) and the wall shear stress (τ_w).

While the integral of the square of the velocity should be derived based on the velocity profile,

$$\overline{v^2} = \frac{1}{\pi R^2}\int_0^R v^2 2\pi r dr \tag{20}$$

Combine Eq. (13) with Eq. (20),

$$\overline{v^2} = \frac{R^2(\tau_w - \tau_0)^{(2/n)+2}}{C^{(2/n)}\tau_w^2((1/n)+2)((1/n)+3)}\left[1 + \frac{6\lambda}{((2/n)+3)} + \frac{((7/n)+9)\lambda^2}{((2/n)+3)((1/n)+1)^2}\right] \tag{21}$$

A correction factor is therefore needed to correct the dynamic part in Eq. (18). In this study, the correction factor will be the ratio between Eqs. (21) and (19):

$$\frac{\overline{v^2}}{\overline{v}^2} = \frac{\left[\begin{array}{c}\frac{1}{((1/n)+2)((1/n)+3)} + \frac{6\lambda}{((1/n)+2)((1/n)+3)((2/n)+3)} \\ + \frac{((7/n)+9)\lambda^2}{((1/n)+2)((1/n)+3)((2/n)+3)((1/n)+1)^2}\end{array}\right]}{\left[\begin{array}{c}\frac{1}{((1/n)+3)^2} + \frac{4\lambda}{((1/n)+2)((1/n)+3)^2} + \frac{4((2/n)+3)\lambda^2}{((1/n)+1)((1/n)+2)^2((1/n)+3)^2} \\ + \frac{8\lambda^3}{((1/n)+1)((1/n)+2)^2((1/n)+3)^2} + \frac{4\lambda^4}{((1/n)+1)^2((1/n)+2)^2((1/n)+3)^2}\end{array}\right]} \tag{22}$$

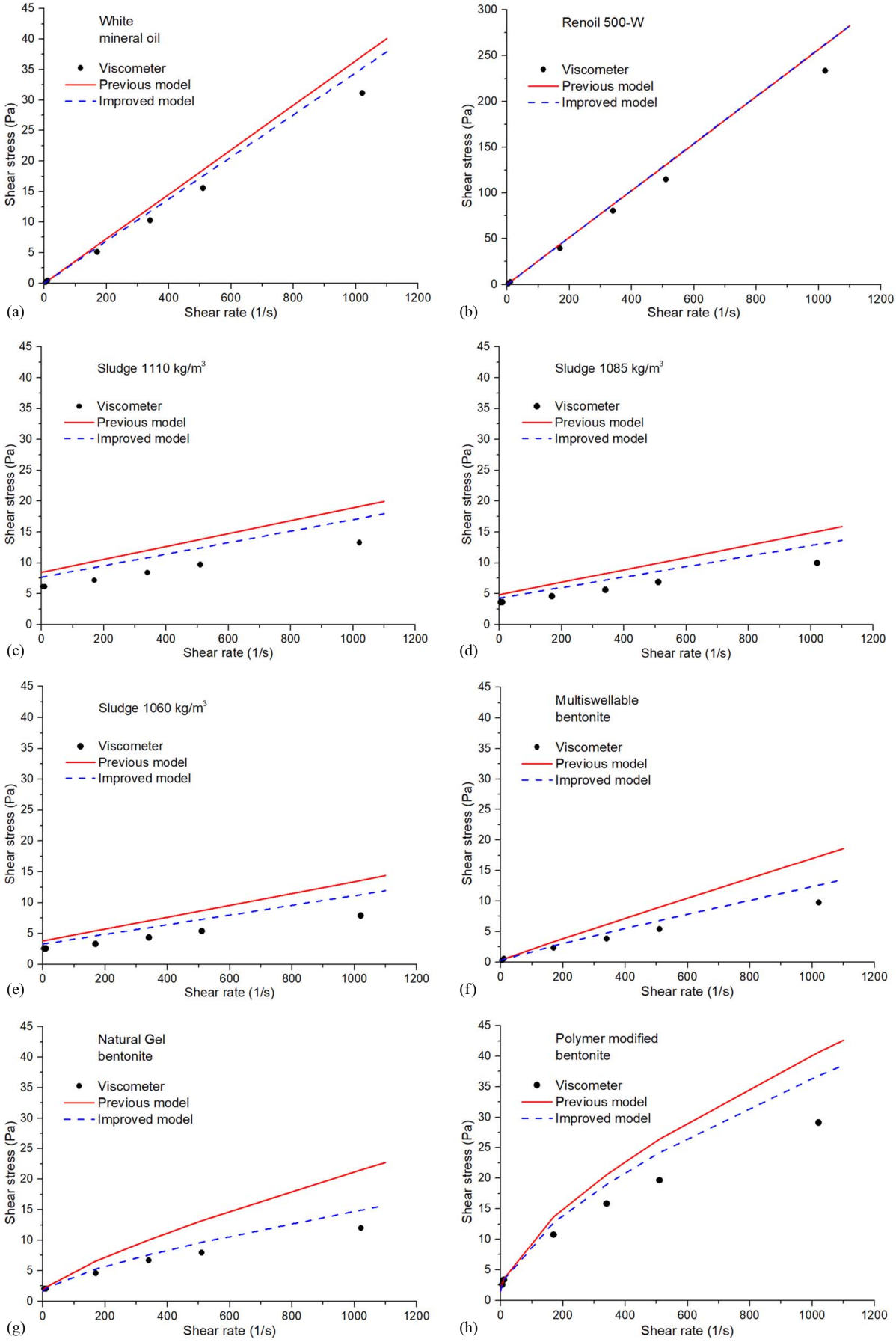

Fig. 9. Consistency plots for: (a) white mineral oil; (b) Renoil 500-W; (c) Sludge 1110 kg/m^3; (d) Sludge 1085 kg/m^3; (e) Sludge 1060 kg/m^3; (f) multiswellable bentonite; (g) natural gel bentonite; and (h) polymer-modified bentonite compared with model results. [Data for (a and b; f–h) from Zheng et al. 2021.]

Eq. (22) suggests that the correction factor depends on the parameters of n and λ. Note that the yield stress (τ_0) should not exceed the wall shear stress (τ_w), suggesting $0 \le \lambda \le 1$.

Fig. 5 shows the correction factor as a function of the ratio between yield stress and wall shear stress for different fluids. It indicates that the correction factor is smaller with a larger λ. The correction factor reduces to 1 when yield stress equals wall shear stress. That makes sense since there will be no shearing among the fluid in that condition, meaning the velocity is the same everywhere in the cross section and it becomes a total plug flow.

The correction factor is smaller in the case of a shear-thinning fluid such as bentonite slurry. However, the yield stress of a bentonite slurry with a small MF viscosity is also small, which makes the correction factor falls within the left part of Fig. 5 where the larger values reside.

The correction factor should be combined with Eq. (18) in order to improve the model prediction, which results as follows:

$$\tau_w = 0.5\frac{R}{L}\left[\Delta P_{tot} - \frac{1}{2}\frac{\overline{v^2}}{\overline{v}^2}\rho\left(\frac{Q}{\pi R^2}\right)^2\right] \tag{23}$$

Results and Discussion

Using the same calculation scheme described by Zheng et al. (2021) and Eq. (23), the improved model prediction can be compared with experimental and previous model results. However, the correction factor should be chosen properly for the non-Newtonian fluids since the wall shear stress is not an explicit value. In this study, the wall shear stress was first determined with the previous model. With the flow index and the ratio between yield stress and wall shear stress, it is possible to get a range of the correction factor using Eq. (22). The average value was taken to be the correction factor for the improved model simulation. The experiments with several Bingham liquids (sludge with different densities) were conducted with the testing system described by Zheng et al. (2021), as shown in Fig. 1(b).

Table 1 shows the parameters found for different fluids. It shows that λ is close to 0 for the considered bentonite slurries due to the small yield stress values. In general, λ is increasing with a larger yield stress. Table 1 shows that the resulting correction factor is located on the left part of Fig. 5, hence it should be taken into consideration.

Fig. 6 shows the results from experiments and model predictions. It shows that the model results are even closer to that of experiments with the correction factor. However, this improvement is barely seen in the results with Renoil 500-W, which is caused by the negligible dynamic force compared with the friction force in the test with the material as indicated by Zheng et al. (2021). As shown in Fig. 7, the dynamic force only dominates in case the MF time is smaller than 50 s. While for those with a larger MF viscosity, the friction force dominates and therefore the improvements on the prediction of the dynamic part will be less significant with an increasing MF value, as shown in Fig. 6.

Although the laminar condition for water could not be determined due to the Reynolds number limitation in this study, the improved model seems to work well when compared with experimental results.

Fig. 8 shows the predicted MF times normalized with the measured MF times for different fluids. It indicates that the improvement on the previous model for the low MF viscosity fluids can be much more effective than for the high MF viscosity fluids. This improvement will decrease as the MF viscosity increases, which is in good compliance with that shown in Fig. 7. Because the improvement will be negligible when the dynamic force is negligible (such as Renoil 500-W), while it will be significant when dynamic force is dominating (such as water).

Fig. 8 also indicates that the prediction ratio of the improved model on Newtonian fluids as well as Bingham fluids used in the study presents a decreasing trend as MF viscosity increases. The prediction ratio for Renoil is around 90%, suggesting an error within 10% for smaller MF viscosity fluids. For shear-thinning fluids (bentonite slurries) used in this study, the prediction ratio also presents a decreasing trend with increasing MF viscosity. It is smaller than the prediction ratio of the fluids with flow index 1. The most probable reason for the large deviations in the shear-thinning fluids ($n < 1$) is the notorious thixotropic property of bentonites slurries for which the shear stress depends on both the shear rate and the shear history (Barnes 1997). For bentonite slurries, the consistency plot will be different when it is obtained by different types of rheometers (Schoesser and Thewes 2015).

By making use of the measured MF time and the total drainage time (which only requires one more testing point for field use), it is possible to get the rheological parameters of the fluid with the previous model. The procedure was also conducted with the improved model.

Fig. 9 shows the consistency plots of different fluids obtained from the model best-fit procedure. The results from the previous model are also included in the figure. It shows that the resulting consistency plots are even closer to the Fann viscometer measurements by introducing the correction factor. Fig. 9 also shows that the improvement is significant for small MF viscosity fluids (such as natural gel bentonite) while negligible for high MF viscosity fluids (such as Renoil 500-W).

Conclusions

This paper introduces an improvement on the previous model that is especially practical for bentonite slurries with small MF values used in tunneling. The velocity profile of the Herschel–Bulkley fluid in a pipe flow suggests that a correction factor should be incorporated owing to the integral value of velocity being unequal to the square value of mean velocity in the previous model. The correction factor is an improvement in the predictions over the dynamic part. Results show that the improvement is significant for fluids with small MF values while negligible for fluids with large MF values. The better performance also shows the advantage of the improved model in the predictions over the rheology parameters of the bentonite slurries. More reliable rheological parameters can be obtained from the improved model with the MF test than from the previous model.

Data Availability Statement

All data, models, and code generated or used during the study appear in the published article.

Notation

The following symbols are used in this paper:

A = cross-sectional area of the pipe;
C = consistency index;
D = diameter of the pipe;
L = length of the fluid;
n = flow index;

P = fluid pressure (corrected for height here in the MF test);
p = dynamic pressure;
Q = discharge;
R = radius of the tube;
Re = Reynolds number;
r = radius of the portion of the fluid;
r_0 = unsheared zone in the flow;
t = measured MF time;
V = drainage volume of 946 mL;
v = fluid velocity;
$\bar{v}$ = mean velocity of the fluid;
$\dot{\gamma}$ = shear rate;
λ = ratio between the yield stress (τ_0) and the wall shear stress (τ_w);
μ = viscosity of the fluid;
ρ = density of the fluid;
ρ_0 = density of water;
τ = shear stress;
τ_0 = yield stress; and
τ_w = wall shear stress.

References

API (American Petroleum Institute). 2009. *Recommended practice for field testing of water-based drilling fluids*. 4th ed. API RP 13B-1. Washington, DC: API.

Balhoff, M. T., L. W. Lake, P. M. Bommer, R. E. Lewis, M. J. Weber, and J. M. Calderin. 2011. "Rheological and yield stress measurements of non-Newtonian fluids using a Marsh funnel." *J. Pet. Sci. Eng.* 77: 393–402. https://doi.org/10.1016/j.petrol.2011.04.008.

Barnes, H. A. 1997. "Thixotropy—A review." *J. Non-Newtonian Fluid Mech.* 70: 1–33. https://doi.org/10.1016/S0377-0257(97)00004-9.

Knisely, C. W., K. Nishihara, and M. Lguchi. 2010. "Critical Reynolds number in constant-acceleration pipe flow from an initial steady laminar state." *J. Fluids Eng.* 132 (9): 091202. https://doi.org/10.1115/1.4002358.

Pitt, M. J. 1999. "The Marsh funnel and drilling fluid viscosity—A new equation for field use." *SPE Drill Completion* 15 (1): 5–8.

Schoesser, B., and M. Thewes. 2015. "Marsh funnel testing for rheology analysis of bentonite slurries for Slurry Shields." In *ITA World Tunnel Congress 2015—SEE Tunnel—Promoting Tunnelling in SEE Region*, 22–28. Dubrovnik, Croatia: Lacroma Valamar Congress Center.

Skelland, A. H. P. 1967. *Non-newtonian flow and heat transfer*. New York: Wiley.

Xiao, Y., Z. Sun, A. M. Stuedlein, C. Wang, Z. Wu, and Z. Zhang. 2020. "Bounding surface plasticity model for stress–strain and grain-crushing behaviors of rockfill materials." *Geosci. Front.* 11 (2): 495–510. https://doi.org/10.1016/j.gsf.2019.06.010.

Xu, T., and A. Bezuijen. 2019. "Bentonite slurry infiltration into sand: Filter cake formation under various conditions." *Géotechnique* 69 (12): 1095–1106. https://doi.org/10.1680/jgeot.18.P.094.

Zheng, D. 2021. "Tunnel boring machine excavation fluids: From laboratory to practice." Ph.D. thesis, Dept. of Civil Engineering, Ghent Univ.

Zheng, D., A. Bezuijen, and G. Di Emidio. 2021. "A new model for predicting the Marsh funnel test." *Int. J. Geomech.* 21 (2): 06020042. https://doi.org/10.1061/(ASCE)GM.1943-5622.0001913.